Photoelectrochemical applications of electrochemical deposition of Ni^{2+}-doped FeS_2 thin films.

PRABUKANTHAN, P., SREEDHAR, M., THAMARAISELVI, S., HARICHANDRAN, G., SEENUVASAKUMARAN, P., HANAFIAH, M.M. and FERNANDEZ, C.

2021

Photoelectrochemical applications of electrochemical deposition of Ni^{2+} doped FeS_2 thin films

P. Prabukanthan[a,*], M. Sreedhar[a], S. Thamaraiselvi[a], G. Harichandran[b], P. Seenuvasakumaran[c] , Marlia M. Hanafiah[d,e], and Carlos Fernandez[f]

[a]Materials Chemistry Lab, Department of Chemistry, Muthurangam Government Arts College, Vellore 632002, India.

[b]Department of Polymer Science, University of Madras, Guindy Campus, Chennai 600025, India

[c]Department of Physics, Muthurangam Government Arts College, Vellore 632002, India.

[d]Department of Earth Sciences and Environment, Faculty of Science and Technology, University Kebangsaan Malaysia, 43600 Bangi, Selangor, Malaysia

[e]Centre for Tropical Climate Change System, Institute of Climate Change, University Kebangsaan Malaysia, 43600 Bangi, Selangor, Malaysia

[f]Department of Chemistry, Robert Gordon University, Aberdeen AB10 7GJ, United Kingdom

Abstract

Different concentration (1–5 mol%) of Ni2+doped FeS2 thin films were deposited by facile ECD technique. XRD pattern Ni2+ ion-doped FeS2 thin films were cubic structure with the high intensity plane (2 0 0). HRSEM images show that the undoped with 1–2 mol% Ni2+ doped FeS2 thin films were spherical-like morphology with aggregated grains. 3 mol% Ni2+ doped FeS2 thin film was aggregated with smaller size grains. Electrochemical impedance analysis reveals that the minimum charge transfer resistance (69 Ω) is obtained for 3 mol% Ni2+ ion-doped FeS2 thin films with exceptional conductivity character compared to other samples. Photoelectrochemical test indicates that 3 mol% Ni2+ ion-doped FeS2 thin film generates enhanced photocurrent response and faster immigration of photoinduced charge carriers compared to the other samples. It has been observed from CV analysis; the optimized 3 mol% Ni2+ doped FeS2 thin film delivers superior electrocatalytic performance of triiodide reduction.

Keywords: Iron pyrite; semiconductor thin films; crystalline nature; photocurrent; electrocatalytic active.

*Corresponding author. Tel.: + 0416-2262068. E-mail address: pprabukanthan76@hotmail.com (P Prabukanthan)

1. Introduction

Recently, several types of materials such as $CulnS_2$, CIGS, CZTS, CdSe, CdTe, FeS_2, played an enhanced performance in photo electrochemical cell. The transition metal ions doped FeS_2 thin films showed an improved performance in photoelectrochemical cell and the substitution is basically good in agreement with the lattice parameters. Among the reported materials, iron disulfide, FeS2 (pyrite) semiconductor compound has been individualized as the most smart photovoltaic material in future with the production oflarge-scale efficient and low cost solar cells. The evolution of pyrite as solar energy materials is because of its nontoxic nature, their abundance and their potential optoelectronic properties. FeS_2 is a well-known earth rich and non-pollutant semiconducting material having wide band gab energy of 0.95 eV. Commonly, FeS_2 showed as much interest in technological importance. It is used as alternative material for photovoltaic and photoelectrochemical cells. FeS_2 thin films showed the different attractive characters such as low production cost, excellent environmental compatibility, ease of n and p doping junction and high carrier mobility [1]. However, by exploring the potential of this material for the solar cell and other photochemical applications finds priority in the recent research field [2-5]. The recent reported results of iron pyrite thin films reveal different potential applications in photoactive electrode [4], dye sensitized solar cells [5], as dilute magnetic semiconductor for spintronics [6], in lithium-ion batteries [7], photo-catalysis [8], as photovoltaic material [9], photo-in electrochemical cells [10] and solar cell devices [11]. As of today, different techniques have been reported for fabrication of FeS_2 thin films such as microwave-irradiation [12], metal organic chemical-vapor deposition (MOCVD) [13], sulfurization of pyrite films [14], magnetic-sputtering [15], chemical bath reaction [17], chemical vapor-deposition[16], electrochemical deposition method [17]. Among the different deposition techniques, the electrochemical deposition is an outstanding method for preparation of FeS_2 thin filmsbecause of an enhanced photoelectrochemical and electrocatalytic performances. This method attracts a considerable attention as this technique is simple, low-cost, environmental friendly, non-pollutant and non-requirement of any modified instrumentation.

Most of the researchers have been reported the various elements (Zn, Ru)-doped pyrite for different potential applications [18-19]. Khalid et al. [20] studied the $M_xFe_{1-x}S_2$ composite for photovoltaic device application through a simple and low cost chemical vapour deposition

(CVD) technique. The prepared FeS_2 thin films employed the bright structural properties and the $M_xFe_{1-x}S_2$ composite has an investigated the Mn-incorporated FeS_2 composite for photoconductivity performance excellent surface morphology deliberate by atomic face microscopy (AFM). Yu et al. [21] have demonstrated a facile chemical bath deposition method and the obtained composite showed enormous light-trapping networks were obtained through increasing doping contents. Ho et al. [22] reported the nickel-incorporated FeS_2 for photoelectrochemical performance through chemical vapor transport (CVT) method and composite displayed excellent single phase with is structural properties. In addition, the nickel doped iron pyrite thin films showed enhanced photoconductive and photoconductivity performance and Ni doped FeS_2 exhibit a fine red shift behavior through reliable with substitutions incorporation.

Jiao et al. [23] have deposited the Co-doped FeS_2 thin films for water photolysis utilizing sunlight by Solvothermal method with enhanced photo response. Starchikov et al. [24] reported the Cr doped $Fe_{1-x}Cr_xS$ single crystalline nanoplates for energy storage devices by a facile thermal decomposition technique. The fabricated Cr doped $Fe_{1-x}Cr_xS$ composite showed the enhanced magnetic properties. This investigation demonstrate that the obtained composite has an attractive material for energy storage devices. Mao et al. [25] reported the $Zn_xFe_{1-x}S_2$ nanocrystals for photoelectrochemical application by a modified hot-injection technique. In this work report that the obtained composited has excellent morphological properties with incorporation of dopant. Thomas et al. [26] reported the $Fe_{1-x}Co_xS_2$ for solar cell application by a simple chemical vapour deposition (MOCVD). The cobalt doped FeS_2 thin films showed a superior conductivity performance and the prepared composite material is suitable for solar cell application.

Jiang et al. studied the Ni-doped FeS_2-rGO electrocatalyst with various composition of Ni (x = 0.05–0.3 mol%) and they found that incorporation of Ni led to yield as better electrocatalyst with lower charge transfer resistance, Tafel slope and lesser reduced over potential [27]. Wang et al. reported that FeS_2/TiO_2 photoanode composed of all earth abundant elements exhibiting high photoresponse for photoelectrochemical cell [28]. On the basis of theoretical and experimental studies, Guo et al. is yet to investigate the electrocatalytic properties of iron chalcogenides in energy conversion storage devices [29]. Xia et al. fabricated Sn^{4+}-doped FeS_2 thin film electrode

for photoelectrochemical materials. They achieved that the Sn^{4+}-doped FeS_2 thin film electrode material has attractive photocurrent density of 0.8 lA cm^{-2} [30]. Predictably, the transition metal ion-doped iron pyrite and their optical properties have been measured individually in relation to diverse tasks. However, the transition metal ion- doped FeS_2 thin films, which combine both electrical and optical properties, seem to be the most novel and remarkable objects for studied not only because of their fundamental properties but also their practical applications in photoelectrochemical cell.

The Ni ions doped thin films for electrochemical properties were infrequently reported. Further, to the best of our knowledge behind the literature review, the transition metal ion-doped FeS_2 thin films were growth on ITO plate through electrochemical deposition (ECD) process and this type of work rarely observed elsewere. The present work, describes the Ni^{2+} ions doped FeS_2 thin films onto ITO plate by a facile and low cost ECD technique. The result of Ni^{2+} on structural, morphological and electrochemical properties of electrochemically deposited FeS_2 thin films was investigated. Moreover, we improved the electrocatalytic performance of Ni^{2+} ion doped FeS_2 thin films and also systematically investigated.

2. Experimental

2.1 Chemicals

In this deposition process, following chemicals such as ferrous sulphate heptahydrate ($FeSO_4.7H_2O$), thiourea ($(NH_2)_2CS$), nickel acetate ($Ni(CH_3COO)_2.xH_2O$) with 3 N purity and tin-doped indium oxide (ITO) substrates were purchased from Sigma-Aldrich, India. Sodium sulfate (Na_2SO_4) with 3 N purity and sulfuric acid (H_2SO_4) were purchased from Spectrochem, India. All of these chemicals were analytical grade and used instantly, voided of any more sanitization.

2.2 Growth of Ni^{2+} doped FeS_2 thin films

The present work illustrates that the undoped and Ni^{2+} ion-doped FeS_2 thin films were grown on ITO coated glass substrate in an electrolyte medium by facile ECD process. In the ECD process, the bath restrained 0.03 mol% dm^{-3} of $FeSO_4.7H_2O$, 0.003 mol% dm^{-3} of ($(NH_2)_2CS$) and the various concentrations (1, 2, 3, 4 and 5 mol%) of Ni^{2+} ions were dissolved by using double distilled water. ECD process was performed by using a linear sweep

voltammetry (LSV) procedure from an electrochemical analyzer (CH604, CH Instrument USA) in three-electrodes setup. An ITO substrate as working electrode, a platinum (Pt) wire contributed as a counter electrode and Ag^{+}/AgCl (saturated KCl) electrode worked as a reference electrode. The resultant solution was magnetically stirred for several minutes at controlled bath in 50°C. ECD bath solution pH (~2) was adjusted by adding conc. H_2SO_4. The LSV for ECD was between -900 mV and +900 mV at a scan rate of 1.5 mVs^{-1}. Further, the formation, the layered thin films were permitted to cool down from higher temperature to room temperature. After completion of ECD process, the deposited thin films were kept in desiccators for further analysis. All the films equipped in this work have average thickness in the range of 386-572 nm.

2.3 Characterization

The structural and crystalline nature of electrodeposited Ni2+ doped FeS2 thin films was investigated by X-ray diffraction (XRD) patterns obtained from Plus/D8 model X-ray diffractometer under Cu Ka radiation at scan rate of 10° per min. Roughness and thickness of electrochemically deposited Ni^{2+} doped FeS_2 thin films were measured by PS50 profilometer system. The resolution of PS50 profilometer system was 5 nm. The surface morphology of samples was tested through high-resolution scanning electron microscope (HRSEM, Hitachi-S-4300SE) with equipped voltage of 10 kV. The optical transmission spectra of the undoped and Ni2+ doped FeS2 thin films were recorded using Shimadzu UV–visible–FIR spectrometer in the range 200–2000 nm. EPR spectra of Ni2+ doped FeS2 thin films were illustrated from Varian E-112 EPR spectrometer at 80 K under liquid nitrogen temperature. A transient photocurrent study was recorded for photo-stability of thin films by using, 100 W Xenon lamps (OSRAM, Germany) which acted as light resource with several on-off cycles in 0.1 M Na_2SO_4 electrolyte solution. The electrochemical impedance spectroscopy (EIS) was examined for Ni^{2+} doped FeS_2 thin films in the frequency range from 0.1 Hz to 1MHz by using AC-impedance technique at AC amplitude of 5 mV at room temperature. The electrocatalytic activity of Ni^{2+} ion-doped FeS_2 thin films were studied by a simple cyclic voltammetry (CV) technique was recorded from CHI604E electrochemical analyzer. Raman spectra of undoped and Ni^{2+} doped FeS_2 thin films were recorded at room temperature. The excitation source was an argon ion laser beam of 30 mW (λ = 488 nm) power with vertical polarization focused to a spot size of 50 mm onto the sample. The scattered light was collected in the backscattering geometry using a camera lens (Nikon; focal

length, 5 cm; f/1.2). The collected light was dispersed in a double grating monochromator, SPEX model 14018, and detected using thermoelectrically cooled photomultiplier tube model ITT-FW 130. The resolution obtained was 5 cm^{-1}. Auger electron spectroscopy (AES) studies were carried out on a Perkin Elmer thin film analyzer using beam current of 180 nA. The experiment is carried out in a UHV environment because the AES technique is surface sensitive due to the limited mean free path of electrons in the kinetic energy range of 2.5 to 3 keV. The pass energy between the deflectors is about 80 eV. Such energy has been chosen because of the good compromise between the resolutions. The spectra were recorded with modulation voltage of 5 eV peak to peak. The samples were sputter etched using a V.G. Scientific ion gun with 3 keV Ar^+ to remove surface contamination. The pressure in the chamber was 5.4 x 10^{-9} Torr during the analysis.

3. Result and Discussion

3.1 Structural, thickness and roughness properties

The structure and crystalline nature of electrochemically deposited thin films were investigated by X-ray diffraction (XRD) performance. Figure 1 shows the characteristic XRD patterns of undoped and various concentrations (1-5 mol%) of Ni^{2+} ion-doped FeS_2 thin films. The observed diffraction peaks matches with the JCPDS Card no. 42-1340 of cubic FeS_2. An enhanced diffraction peaks with the related planes of (2 0 0), (2 1 0) and (2 2 1) are of well crystalline in character with cubic structure. The major diffraction peak of (2 0 0) plane shows the highest intensity by exhibiting the cubic structure with preferred orientation. The observed diffraction peaks are slightly shifted to lower 2θ degree which is due to larger ionic radius of Ni^{2+} (0.083 nm) ions substituted in the smaller Fe^{2+} (0.074 nm) lattice sites and also the atoms located in the lattice boundaries is considerably changed. The results clearly indicate that there is a significant change in diffraction peaks and the successful Ni^{2+} doping in the host FeS_2 matrix [31]. The 2, 3 and 4 mol% of Ni^{2+} doped FeS_2 thin films have additional diffraction peaks of (2 1 1) and(2 2 0) appeared. The lattice constant (a) of thin films were estimated from the (h k l) planes and described in the following relation,

$$a = d\,(h^2 + k^2 + l^2)^{1/2} \quad (1)$$

where d is inter planar spacing for atomic planes. The obtained d-spacing values are used to resolve the lattice constant and values are summarized in Table 1. The average crystallite size (D) of thin films was estimated by FWHM of (2 0 0) diffraction peak using Scherer's equation:

$$D = 0.9\,\lambda/\beta\cos\theta \quad (2)$$

where β is the full width at half maximum (in radians) and λ is the X-ray wavelength. The estimated, average crystallite sizes were in the range of 101-190 nm and agreed in Table 1. The microstrain (ε), dislocation density (δ) and number of crystallites per unit area (N) were determined by using following relations (Eqs. 3, 4 and 5) and their values are summarized in Table 1.

$$\text{Micro strain } (\varepsilon) = \beta\cos\theta/4 \quad (3)$$

$$\text{Dislocation density } (\delta) = 15\varepsilon/aD \quad (4)$$

$$\text{Number of crystallites } (N) = t/D^3 \quad (5)$$

where θ is the Bragg's angle (in degree), t is thickness of the film, ε and δ are very regular physical phenomena for thin films. The obtained strain (ε) value induces that the deformation of one part per million.

The thickness and roughness values of undoped and Ni^{2+} ion-doped FeS_2 thin films were obtained by profilometry process and the values are given in Table 2. While the thicknesses and roughness of 1, 2, 3, 4 and 5 mol% Ni^{2+} doped thin films are higher than that of undoped thin films, the roughness values are lower than that of undoped thin films. This may be due to faster particle growth in the presence of Ni^{2+} ions leading to better crystallization of the product.

3.2 Surface morphology studies

The microstructure and surface morphology of electrodeposited undoped and Ni^{2+} ion-doped FeS_2 thin films were performed by using high resolution scanning electron microscopy (HRSEM). The Figure 2 gives the typical HRSEM surface images of undoped and 1-5 mol% of Ni^{2+} ion-doped FeS_2 thin films. The HRSEM images obviously indicates that the Ni^{2+} ions concentration display a significant role on the surface morphology and grain size of the thin films. The surface morphology of undoped (Figure 2 a) FeS_2 thin film show a smaller grain with

uneven spherical-like structure. After increasing doping concentrations (1-2 mol%), the HRSEM (Figure 2 b-d) images reveal spherical-like morphology with gradual increase in uniform-sized aggregated grains. The morphology of 3 mol% Ni^{2+} ion-doped FeS_2 thin films is relatively small and quite different from other thin films. Its agglomerated nanocrystalline particles were distributed on the surface. From the illustration, it is observed that the all thin films showed a homogeneous, without cracks or pinholes and well covered to the ITO glass substrates. The case of 4 mol% Ni^{2+} ion-doped FeS_2 thin film shows a series of aggregated grains with irregular bigger crystallites, and grain size was increased with increasing Ni^{2+}-dopant concentration. Reaching the dopant concentration (5 mol%) of Ni^{2+} ion-doped thin films displayed the spherical-like morphology and slightly reduced grains with even distribution of grains. The increase in grain size suggests that the crystallinity of thin film was enhanced. The results suggest that the decrease of grain boundary may be due to the good adhesion in nature of thin films with increase in conductivity of the samples [32]. As the particle size decreases, the number of surface volume increases, so that nickel additive is segregated over FeS_2 surface.

3.3 Optical studies

Figure 3 shows the Tauc's relation plotted against (αhγ)2 and (hγc) of pure and Ni^{2+} doped FeS_2 thin films. The as-deposited undoped and 1, 2 mol% of Ni^{2+} doped FeS_2 thin films should be a sharp absorption coefficient edge and observed bandgap were 0.9538, 0.9479, and 0.9442 eV. The absorption coefficient edge was not sharp and band were 0.9384, 0.9312 and 0.9301 eV for 3, 4 and 5 mol% Ni^{2+} doped FeS_2 thin films. The obtained energy gap is slightly reduced which might be because the dopant effectively substituted into the FeS_2 lattice and cubic phase-induced lattice damage creates defect energy levels below the conduction band. Decreasing of energy gap increases Ni^{2+} in the FeS_2, which employed the interactions of sp-d exchange among the band electrons in FeS_2 and the localized d electrons of the Ni^{2+} ions [2, 17].

3.4 EPR Studies

The state of nickel ions and local environmental interactions are studied by using electron paramagnetic resonance (EPR). Figure 4 shows that EPR spectra of Ni^{2+} ions (1-5 mol%)-doped FeS_2 thin films at liquid nitrogen temperature (LNT). FeS_2 is low spin compound with diamagnetic nature and EPR inactive. However, the Ni^{2+} ions are substituted into Fe^{2+} sites of

FeS_2 thin films and the +2 charge state correspond to $3d^8$ configurations. The EPR spectra of Ni^{2+} ions are octahedral in nature with an effective spin value of 1, which happens from the splitting of the ^3F ground term symbol, the EPR result observed the doublet. The EPR spectra of Ni^{2+} doped FeS_2 thin film show a weaker peak centered at 154-156 mT ($g_x = g_y = 4.297$) and sharp enhanced peak centered at 349, 351, 352, 354 and 430 mT ($g_z = 1.928$), for Ni^{2+} ions (1-5 mol%)-doped FeS_2 thin films, respectively. The obtained lines are attributed to the perpendicular and parallel components corresponding to octahedrally coordinate with paramagnetic of Ni^{2+} ions incorporated at Fe^{2+} sites into the cubic FeS_2 system. It indicates that the octahedral symmetry is distorted little axially. When reached the Ni^{2+} ions concentration from 1 to 3 mol%, it is observed the higher distortion of the lattice resultant in the relocation of electron charge around Ni^{2+}ions [17]. It can be seen that the intensity of the ~354 mT signal increases with increasing Ni^{2+}concentration capable of 3 mole %, besides the intensity reduce due to the large concentration of Ni^{2+} ions.

3.5 Electrochemical impedance spectroscopy studies

The electrochemical impedance spectroscopy (EIS) of undoped and Ni^{2+} ion-doped FeS_2 thin films was examined by using Nyquist and admittance plots. The obtained Nyquist plots are characterized for frequency response of the electrode/electrolyte system with the plots of the imaginary component (−Z) of the impedance against the real component (Z). The Nyquist plots for undoped and the Ni-doped FeS_2 thin films were given in Figure.5. The admittance plot of Ni^{2+} ion-doped FeS_2 thin films were given in Figure 6. The calculated values of solution resistance (R_s), charge transfer resistance (R_{ct}) and bulk resistance (R_b) are summarized in Table 2. In addition, the diameter of semicircle is indicated that the charge transfer resistance (R_{ct}) of the Ni^{2+} ion-doped thin films with the electrolyte interfaces. However, the observed results of semicircle radius and charge transfer resistance (R_{ct}) for 3 mol% of Ni^{2+} ion-doped FeS_2 thin film were observed to be very low (R_{ct} is 69 Ω). This implies that the 3 mol% of Ni^{2+} ion-doped FeS_2 thin film employed the better electron transfer between electrode/electrolytes and fine conductivity compared to the other samples, which may be due to the Ni^{2+} ions into the FeS_2 host lattice [33]. The lower charge transfer resistance (R_{ct}) value indicates that the film exhibits higher ionic conductivity, which may ensure the feasibility of their role in electrochemical device application.

3.6 Photoelectrochemical studies

The photoelectrochemical analysis was recorded for the transient photocurrent response of thin films and which also gives the supporting information of the electrochemical properties of Ni^{2+} ion-doped FeS_2 thin films. The transient photocurrent response of the undoped and Ni^{2+} ion-doped FeS_2 thin films were performed with light on/off cycles under visible light irradiation and the results are found in Figure 7. The observed results demonstrated that the 3 mol% of Ni^{2+} ion-doped FeS_2 thin films generates enhanced photocurrent response compared to the other samples, which indicates that the charge separation efficiency of 3 mol% of Ni^{2+} ion-doped FeS_2 thin film is slightly higher to produce more photoinduced charge carriers performance. In addition, the undoped FeS_2 thin film photocurrent density of 0.9814 μAcm^{-2} is lower compared to the other samples, which indicates that the doping of Ni^{2+} ions could develop the photocurrent performance obviously. Moreover, the obtained results demonstrated that the 3 mol% of Ni^{2+} ion-doped FeS_2 thin film was produced exceptionally, with better characteristic properties and the best potential candidate for photoelectrochemical device applications [32]. The photocurrent of the pure and Ni^{2+} doped FeS_2 thin films photoanode reached saturation very fast, representing the less surface traps in the pure and N^{2+} doped FeS_2 film.

3.7 Electrocatalytic activity

The electrocatalytic activity of electrochemically deposited Ni^{2+} doped FeS_2 thin films was studied by using a facile cyclic voltammetry (CV) technique in an aqueous electrolyte medium. The Figure 8 shows the catalytic activity of undoped and the Ni^{2+} ions (1-5 mol %)-doped FeS_2 thin films were recorded with the I^-/I^-_3 redox couple. The CV curves were scanned in three-electrode system with the Ni^{2+} doped FeS_2 thin film as a working electrodes, the Pt wire as a counter electrode and saturated calomel (Ag^+/AgCl/KCl) electrode served as a reference electrode. However, the characteristic peaks of Ox-1 and Red-1(negative potential) are focused for the analysis of CEs is responsible for catalyzing the reduction of I^-_3 to I^- ions. Also, the left pair of peaks at lower potential (oxidation-1 and reduction-1) appeared to the oxidation and reduction in iodide/triiodide and according to equation 6, beside the right pair of peaks in higher potential (Ox-2 and Red-2) was recognized to the redox reaction shown in equation 7.

$$I^-_3 + 2e^- \Leftrightarrow 3I^- \quad (6)$$

$$3I^- + 2e^- \Leftrightarrow I^-_3 \quad (7)$$

The observed peak current density (IPC) and the peak-to-peak separation (EPP) are significant factors for estimating to the electrocatalytic activity of various CE [33]. Furthermore, the peak current density is used to estimate the catalytic activity of the counter electrodes. Figure 9 employs the observed catalytic activity of 3 mol% of Ni^{2+} ion-doped FeS_2 thin film is better than that of Pt electrode for its higher peak current density. From this result, we suggest that 3 mol% of Ni^{2+} ion-doped FeS_2 thin film could be used as a substitution electrode material for electrochemical device application.

3.8 Raman spectra studies

The Raman spectra of the undoped and Ni^{2+} doped FeS2 thin films are shown in Fig. 10a–f. Figure 10 shows three peaks at 341, 377 and 427 cm^{-1} and the high intensity peak (377 cm-1) in the pyrite structure with in-phase stretching vibration of S–S (Ag). The other two low intensity peaks (341 and 427 cm^{-1}) are the characteristic active modes for pyrite corresponding to the S_2 dumb bell liberation with Fe–S atom displacements perpendicular to the molecular axis (E_g) and coupled liberation and stretching vibration (T_g) modes, respectively [17, 30]. When Ni^{2+} doped FeS_2 thin films, the E_g and T_g modes are noticeably broadened and decreased intensity with increasing nickel concentrations. It may be due to large lattice strain, static disorder and thermal vibrational disorder of the material. The high intensity peak Ag was splitting in doublet for 4 and 5 mol% Ni^{2+} doped FeS_2 thin films, indicating that the Ni^{2+} substitutes stoichiometrically for Fe^{2+} on the iron pyrite lattice and existence of the mass effect with electronegativity difference effect. This further confirms that Ni^{2+} has been doped into the FeS_2 crystal lattice (Fig. 10).

3.9 Auger electron spectroscopy (AES) studies

The atomic concentration of iron, sulfur and nickel were obtained using auger electron spectroscopy (AES). The AES depth profile of pure, 3 and 5 mol% Ni^{2+} doped FeS_2 thin films as shown in Fig. 11a–c shows that there is deviation in the compositions of iron, when the nickel concentration in FeS_2 thin films. So these results indicate that nickel might act as a substitute at iron lattice site in the FeS_2 thin films. The 5 mol% Ni^{2+} doped FeS_2 thin film showed a high concentration of nickel atom which was due to the addition of more nickel source and also to maintain stoichiometric.

4. Conclusion

Ni^{2+} ions (1-5 mol%) doped FeS_2 thin films were successfully deposited on ITO substrates through a simple ECD route. X-ray diffraction (XRD) studies reveals that, Ni^{2+} ion-doped FeS_2 thin films exhibit a cubic structure with preferential orientation along (2 0 0) plane as a higher peak. HRSEM surface morphology studies reveals that 1-3 mol% $Ni2^{+}$ ion-doped FeS_2 thin films showed spherical-like morphology with aggregated grains. When the doping concentration is increased to 4 mol%, the thin film shows a series of aggregated grains and on further increasing the doping to 5 mol%, the thin films exhibit spherical-like morphology with slightly reduced grains. The decrease in bandgap energy on doping of Ni^{2+} ions may be due to modification in stoichiometry and also change in crystallite size. EPR spectra revealed that the Ni^{2+} ion-doped FeS_2 thin films display a weaker peak, while sharp enhanced peaks are observed for 1-5 mol% Ni^{2+} ion-doped FeS_2 thin films. EIS test reveals that the 3 mol% Ni^{2+} ion-doped FeS_2 thin films shows tiny charge transfer resistance (69 Ω) compare to other samples with good conductivity nature. From the photoelectrochemical analysis it has found that 3 mol% Ni^{2+} ions (3 mole%)-doped FeS_2 thin films exhibited the quicker immigration of photoinduced charge carriers compare to other samples. Moreover, cyclic voltammetry (CV) studies reveals a fact that the optimized 3 mol% of Ni^{2+} doped FeS_2 thin film shows better electrocatalytic performance under triiodide reduction. From the experimental results we may come to a conclusion that the 3 mol% Ni^{2+} ion-doped FeS_2 thin films could be a well-optimistic resource material for photoelectrochemical device applications. Optical absorption, Raman spectra and AES studies showed that Ni^{2+} are substituted in the Fe^{2+} sites of the FeS_2 crystal host lattice.

Acknowledgements

The author Dr. P. Prabukanthan would like to acknowledge the University Grant Commission (UGC), India, for the financialassistance through major research project (MRP) scheme [File No.43-399/2014(SR)].

Reference

1. Z. Shi, A.H. Jayatissa, F.C. Peiris, Fabrication of semicon- ducting pyrite thin films from hydrothermally synthesized pyrite (FeS2) powder. J. Mater. Sci. 27, 535–542 (2016). https://doi.org/10.1007/s10854-015-3786-5
2. P. Prabukanthan, R. Lakshmi, G. Harichandran, T. Tatarchuk,Photovoltaic device performance of pure, manganese (Mn2?) doped and irradiated CuInSe2 thin films. New J. Chem. 42, 11642–11652 (2018). https://doi.org/10.1039/C8NJ01056K
3. P. Prabukanthan, R.J. Soukup, N.J. Ianno, A. Sarkar, C.A. Kamler, E.L. Extrom, J. Olejnicek, S.A. Darveau, Chemical bath deposition (CBD) of iron sulfide thin films for photovoltaic applications, crystallographic and optical prop- erties. in: Proceedings of the 35th Photovoltaics specialists Conference, Institute of Electrical and Electronics Engineers (IEEE) 002965–002969 (2010). https://doi.org/10.1109/PVS C.2010.5614465
4. D.G. Moon, S. Rehana, S.Y. Lim, D. Nam, Structural, optical and electrical impacts of marcasite in pyrite thin films. Sol. Energy 159, 930–939 (2018). https://doi.org/10.1016/j.solene r.2017.11.026
5. D. Ma, J. Zai, Y. Wang, Q. Qiao, X. Qian, Fe1-xCoxS2 solid solutions with tunable energy structures to enhance the per- formance of triiodide reduction in dye-sensitized solar cells. Chem. Nano Mater. 4, 1043–1047 (2018). https://doi.org/10.1002/cnma.201800247
6. Zutic, J. Fabian, S. Das Sarma, Spintronics: fundamentals and applications. Rev. Mod. Phys. 76, 323–410 (2004). https://doi.org/10.1103/RevModPhys.76.323
7. B. Thomas, T. Cibik, C. Ho¨ pfner, Formation of secondary iron-sulphur phases during the growth of polycrystalline iron pyrite (FeS2) thin films by MOCVD. J. Mater. Sci. 9, 61–64 (1998). https://doi.org/10.1023/A:1008943203807
8. S. Bae, D. Kim, W. Lee, Degradation of diclofenac by pyrite catalyzed fentonoxidation. Appl. Catal. B. 134, 93–102 (2013). https://doi.org/10.1016/j.apcatb.2012.12.031
9. P. Prabukanthan, S. Thamaraiselvi, G. Harichandran, Structural, morphological, electrocatalytic activity and photocurrent properties of electrochemically deposited FeS2 thin films. J. Mater. Sci. 29, 11951–11963 (2018). https://doi.org/10.1007/s10854-018-9297-4
10. S.L. Liu, M.M. Li, S. Li, H.L. Li, L. Yan, Synthesis and adsorption/photocatalysis performance of pyrite FeS2. Appl. Surf. Sci. 268, 213–217 (2013). https://doi.org/10.1016/j.aps usc.2012.12.061
11. S. Shukla, J.W. Ager, Q. Xiong, T. Sritharan, Scientific and technological assessment of iron pyrite for use in solar devices. Energy Technol. 6, 8–20 (2017). https://doi.org/10.1002/ente.201700638
12. E.J. Kim, B. Batchelor, Synthesis and characterization of pyrite (FeS2) using microwave irradiation. Mater. Res. Bull. 44, 1553–1558 (2009). https://doi.org/10.1016/j.materresbull.2009.02.006
13. G. Chatzitheodrou, S. Fiechter, M. Kunst, W. Jaegermann, H. Tributsch, Thin photoactive FeS2 (pyrite) films. Mater. Res. Bull. 21, 1481–1487 (1986). https://doi.org/10.1016/0025-5408(86)90088-7
14. A.M. Huerta-Flores, J.M. Mora-Herna´ndez, L.M. Torres- Mart´ınez, Extended visible light harvesting and boosted charge carrier dynamics in heterostructured

zirconate–FeS2 photocatalysts for efficient solar water splitting. J. Mater. Sci. 29, 18957–18970 (2018). https://doi.org/10.1007/s10854-018-0019-8
15. D. Lichtenberger, K. Ellmer, R. Schieck, S. Fiechter, H. Tri- butsch, Structural, optical and electrical properties of poly- crystalline iron pyrite layers deposited by reactive DC magnetron sputtering. Thin Solid Films 246, 6–12 (1994). https://doi.org/10.1016/0040-6090(94)90723-4
16. S.D. Disale, S.S. Garje, Deposition of copper doped iron sulfide (CuxFe1–xS2) thin films using aerosol-assisted chemi- cal vapor deposition technique. Appl. Organometal. Chem. 24, 734–740 (2010). https://doi.org/10.1002/aoc.1676
17. P. Prabukanthan, S. Thamaraiselvi, G. Harichandran, Single step electrochemical deposition of p-type undoped and Co2? doped FeS2 thin films and performance in heterojunction solid solar cells. J. Electrochem. Soc. 164, D581–D589 (2017). https://doi.org/10.1149/2.0991709jes
18. P. Xiao, X. Fan, H. Zhang, X. Fang, L. Liu, Increasing the band gap of FeS2 by alloying with Zn and applying biaxial strain: a first-principles study. J. Alloy Compd. 629, 43–48 (2015). https://doi.org/10.1016/j.jallcom.2014.11.217
19. B. Ouertani, H. Ezzaouia, Bertr, effect of ruthenium alloy on the band gap value of FeS2-pyrite. Colloids Surf. 525, 13–19 (2017). https://doi.org/10.1016/j.colsurfa.2017.04.038
20. S. Khalid, M. Azad, M. David, J. Lewis, P. Kevin, E. Ahmed, Y. Khanc, P. Brienad, Transition metal doped pyrite (FeS2) thin films: structural properties and evaluation of optical band gap energies. J. Mater. Chem. C 3, 12068–12076 (2015). https://doi.org/10.1039/C5TC03275J
21. Q. Yu, S. Cai, Z. Jin, Z. Yan, Evolutions of composition, micro- structure and optical properties of Mn doped pyrite (FeS2) films prepared by chemical bath deposition. Mater. Res. Bull. 48, 3601–3606 (2013). https://doi.org/10.1016/j.materresbull.2013.05.074
22. C.H. Ho, C.E. Huang, C.C. Wu, Preparation and characterization of Ni-incorporated FeS2 single crystals. J. Crystal Growth 270, 535–541 (2004). https://doi.org/10.1016/j.jcrysg ro.2004.07.017
23. J. Jiao, L. Chen, D. Kuang, W. Gao, H. Feng, J. Xia, Syn- thesis of FeS2 and Co-doped FeS2 films with the aid of supercritical carbon dioxide and their photoelectrochemical properties. RSC Adv. 1, 255–261 (2011). https://doi.org/10.1039/C1RA00066G
24. S.S. Starchikov, I.S. Lyubutin, C.-R. Lin, Y.-T. Tseng, K.O. Funtov, Y.L. Ogarkova, T.V. Dmitrieva, A.G. Ivanova, Synthesis and magnetic properties of the chromium doped iron sulfide Fe1-xCrxS2 single crystalline nanoplates with a NiAs crystal structure. Phys. Chem. Chem. Phys. 17, 15829–15836 (2015). https://doi.org/10.1039/C5CP01846C
25. B. Mao, Q. Dong, Z. Xiao, C.L. Exstrom, S.A. Darveau, T.E. Webber, B.D. Lund, H. Huang, Z. Kang, J. Huang, Zinc alloyed iron pyrite ternary nanocrystals for band gap broadening. J. Mater. Chem. A. 1, 12060–12065 (2013). https://doi.org/10.1039/C3TA11039G
26. B. Thomas, K. Ellmer, W. Bohne, J. Rohrich, M. Kunst, H. Tributsch, Photoeffects in cobalt doped pyrite (FeS2) films. Solid State Commun. 111, 235–240 (1999). https://doi.org/10.1016/S0038-1098(99)00213-6
27. J. Jiang, L. Zhu, H. Chen, Y. Sun, H. Lin, S. Han, Effect of nickeldoped FeS2 Nanoparticles-reduced graphene oxide electrocatalysts for efficient hydrogen evolution. J. Alloys Compd. 775, 1293–1300 (2019). https://doi.org/10.1016/j.ja llcom.2018.10.261

28. D.-Y. Wang, C.-H. Li, S.-S. Li, T.-R. Kuo, C.-M. Tsai, T.R. Chen, Y.-C. Wang, C.-W. Chen, C.-C. Chen, Iron pyrite/titanium dioxide photoanode for extended near infrared light harvesting in a photoelectrochemical cell. Sci. Rep. 6, 20397 (2016). https://doi.org/10.1038/srep20397
29. J. Guo, S. Liang, Y. Shi, Bo. Li, Ce. Hao, X. Wang, T. Ma, Electrocatalytic properties of iron chalcogenides as low-cost counter electrode materials for dye-sensitized solar cells. RSC Adv. 5, 72553–72561 (2015). https://doi.org/10.1039/C5RA13147B
30. J. Xia, X. Lu, W. Gao, J. Jiao, H. Feng, L. Chen, Hydrothermal growth of Sn4? doped FeS2 cubes on FTO substrates and its photoelectrochemical properties. Electrochim. Acta 56, 6932–6939 (2011). https://doi.org/10. 1016/j.electacta.2011.06.021
31. R.J. Soukup, P. Prabukanthan, N.J. Ianno, A. Sarkar, C.A. Kamler, D.G. Sekora, Formation of pyrite (FeS2) thin films by thermal sulfurization magnetron sputtered iron. J. Vac. Sci. Technol. A. 29, 011001 (2011). https://doi.org/10.1116/1.3517739
32. T. Rajesh Kumar, P. Prabukanthan, G. Harichandran, J. Theerthagiri, A. Meera Moydeen, G. Durai, P. Kuppusami, T. Tatarchuk, Comparative study of structural, optical and electrical properties of electrochemically deposited Eu, Sm and Gd doped ZnSe thin films. J. Mater. Sci. Mater. Electron. 29, 5638–5648 (2018). https://doi.org/10.1007/s10854-018-8 533-2
33. P. Prabukanthan, S. Thamaraiselvi, G. Harichandran, J. Theerthagiri, Single-step electrochemical deposition of Mn2? doped FeS2 thin films on ITO conducting glass substrates: physical, electrochemical and electrocatalytic properties. J. Mater. Sci. 30, 3268–3276 (2019). https://doi.org/10.1007/s10854-018-00599-w

Figure captions

Figure 1(a-f) XRD patterns of the as-deposited (a) undoped FeS_2 and Ni^{2+} ions doped FeS_2 thin films (b) 1 mole %, (c) 2 mole %, (d) 3 mole %, (e) 4 mole % and (f) 5 mole %.

Figure 2(a-f) HRSEM images of as-deposited a) undoped FeS_2 and Ni^{2+} ions doped FeS_2 thin films (b) 1 mole %, (c) 2 mole %, (d) 3 mole %, (e) 4 mole % and (f) 5 mole

Figure 3 Absorption coefficient vs photon energy spectra of pure and Ni2+doped FeS2 films

Figure 4 EPR spectra for the undoped and Ni^{2+} ions (1-5 mole %) doped FeS_2 thin films.

Figure 5 Nyquist plots for the undoped and Ni^{2+} ions (1-5 mole %) doped FeS_2 thin films.

Figure 6 Nyquist admittance for Ni^{2+} ions (1-5 mole %) doped FeS_2 thin films.

Figure 7 Transient photo-current response of undoped and Ni^{2+} ions (1-5 mole %) doped FeS_2 thin films in visible light irradiation.

Figure 8 Cyclic voltammogram curves of undoped and Ni^{2+} ions doped FeS_2 thin films.

Figure 9 Cyclic voltammogram curves of Pt and 3 mole % of Ni^{2+} ions doped FeS_2 Thin films.

Figure 10 Raman spectra of the as-deposited a undoped FeS_2 and Ni^{2+} ion-doped FeS_2 thin films b 1 mol%, c 2 mol%, d 3 mol%, e 4 mol% and f 5 mol

Figure 11(a-c) Auger electron spectroscopy of a undoped FeS_2, b 3 mol% Ni^{2+} doped FeS_2 and c 5 mol% Ni^{2+} doped FeS_2 thin films

Table Captions

Table.1 FWHM, Crystallite size, Micro strain, Dislocation density, Number of crystallites per unit area of undoped and Ni^{2+} ion doped FeS_2 thin films

Table.2 Thickness, roughness and electrochemical impedance performance calculated data of undoped and Ni^{2+} ion doped FeS_2 thin films.

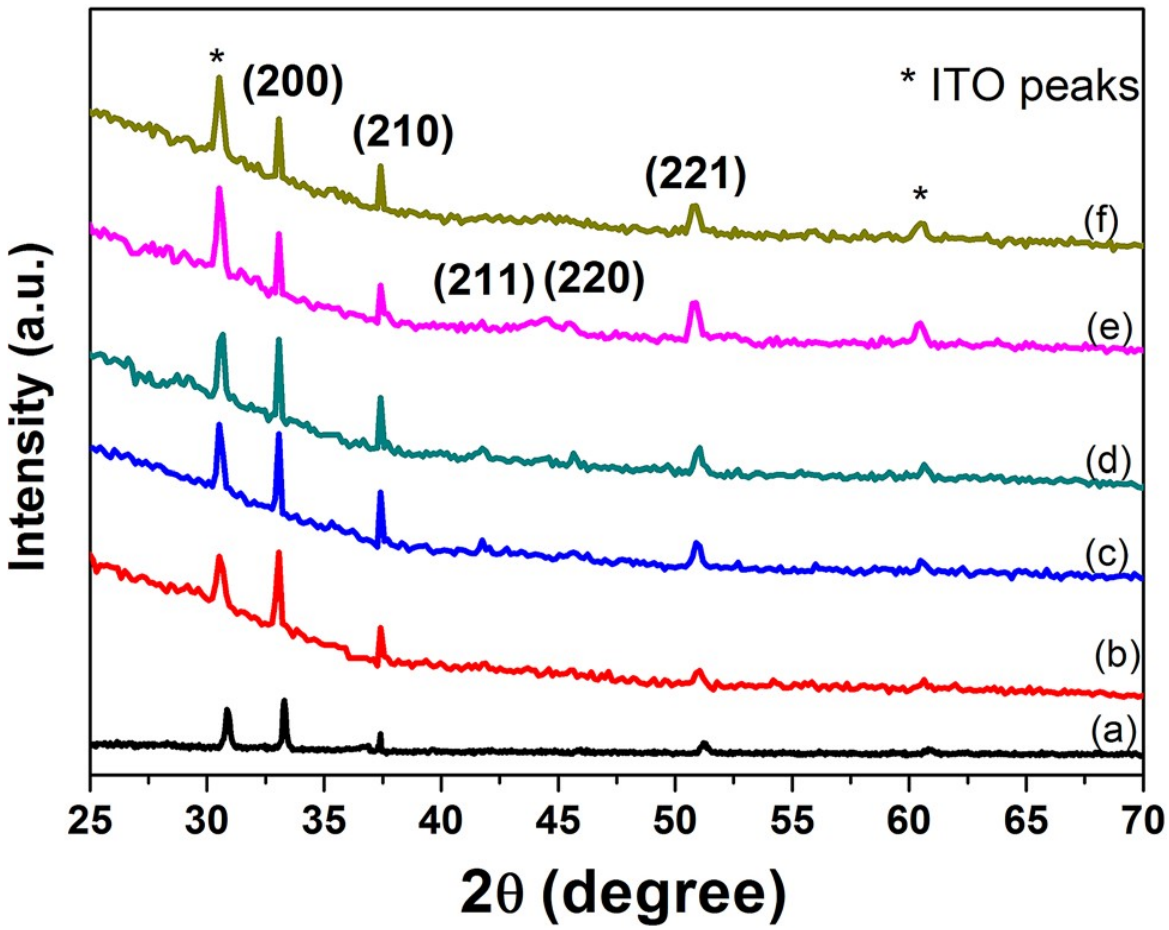
* (200)
(210)
(221)
*
* ITO peaks
(f)
(211) (220)
(e)
(d)
(c)
(b)
(a)
Intensity (a.u.)
25 30 35 40 45 50 55 60 65 70
2θ (degree)

Figure 1(a-f)

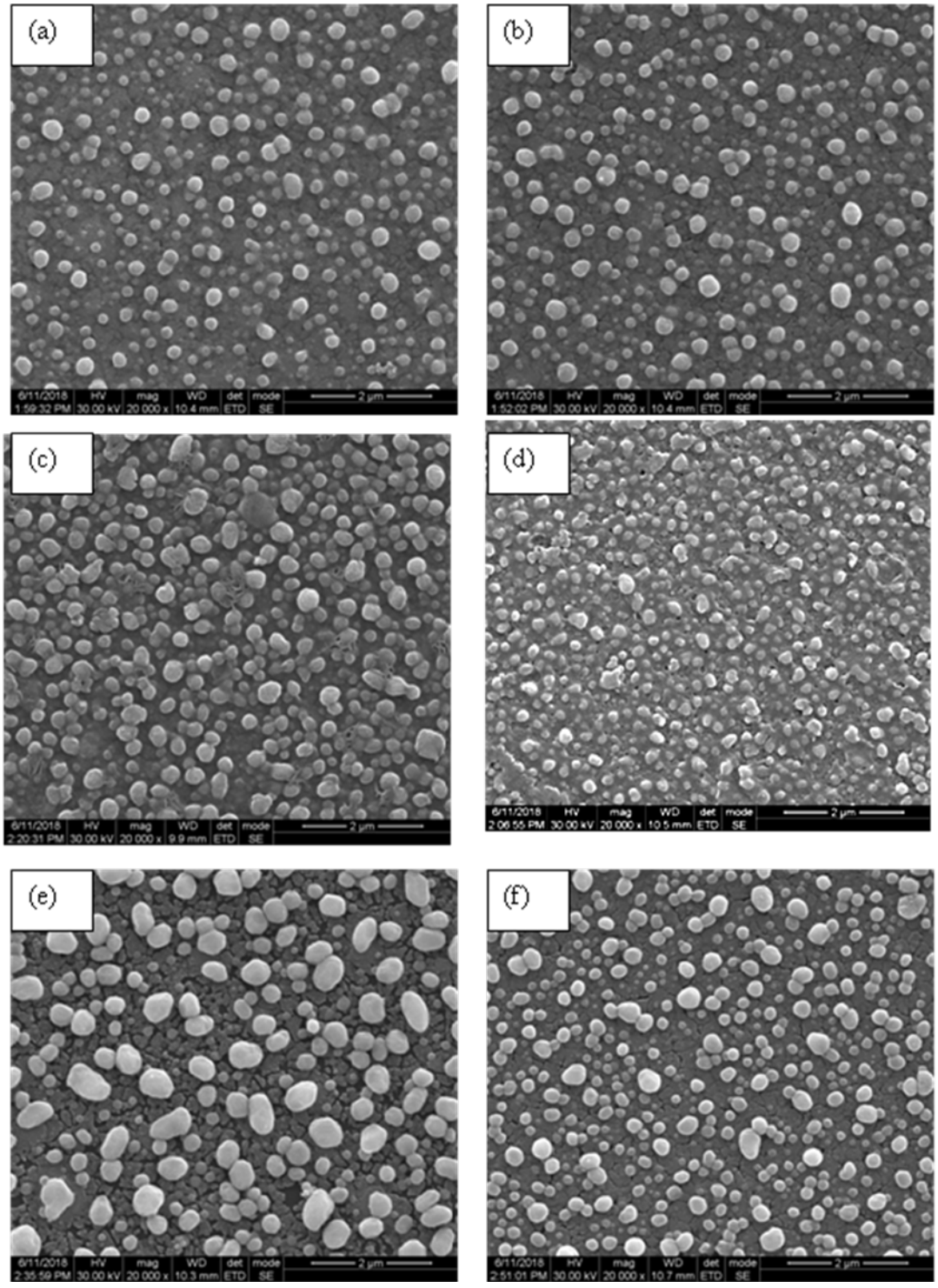

Figure 2 (a-f)

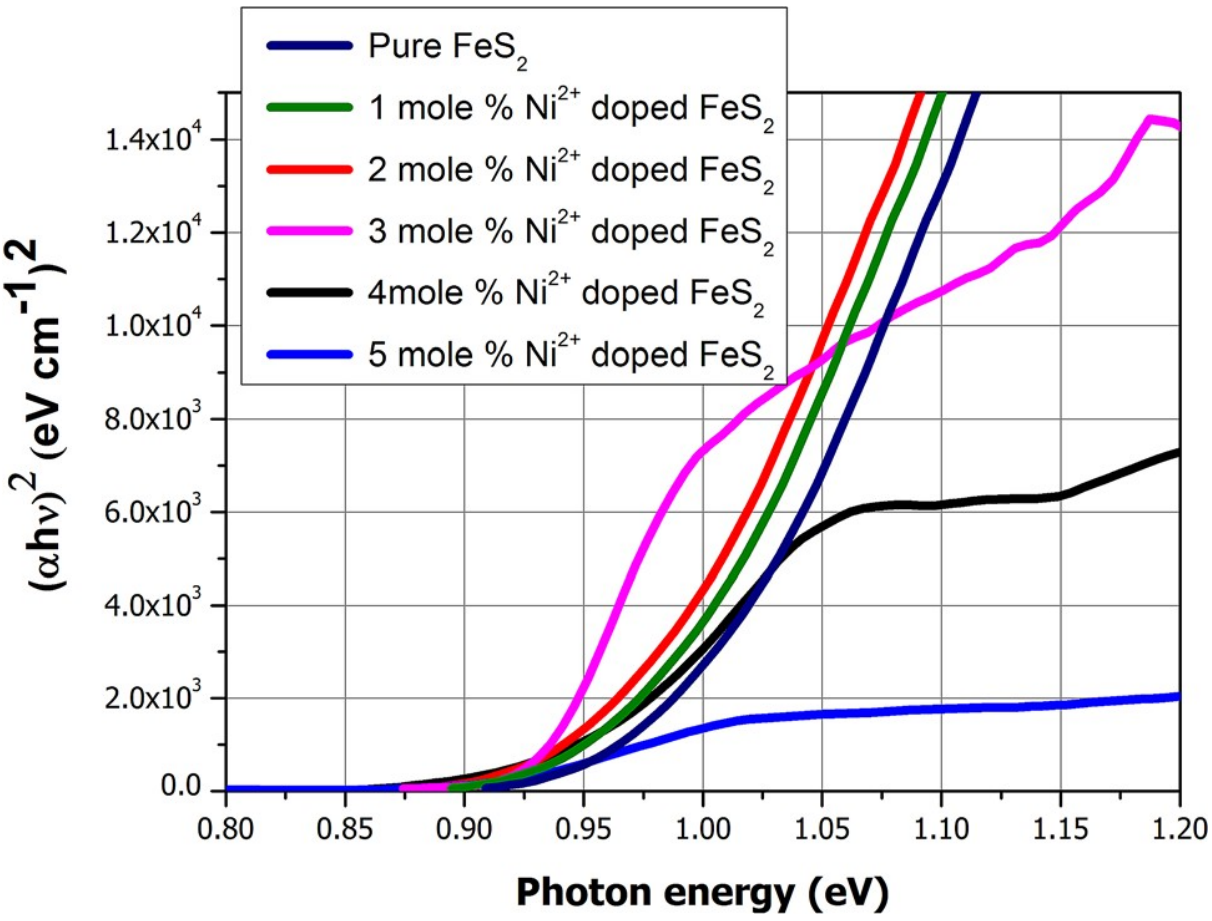
Pure FeS2
1 mole % Ni2+ doped FeS2
2 mole % Ni2+ doped FeS2
3 mole % Ni2+ doped FeS2
4mole % Ni2+ doped FeS2
5 mole % Ni2+ doped FeS2
(αhν)2 (eV cm-1)2
1.4x10^4
1.2x10^4
1.0x10^4
8.0x10^3
6.0x10^3
4.0x10^3
2.0x10^3
0.0
0.80
0.85
0.90
0.95
1.00
1.05
1.10
1.15
1.20
Photon energy (eV)

Figure 3

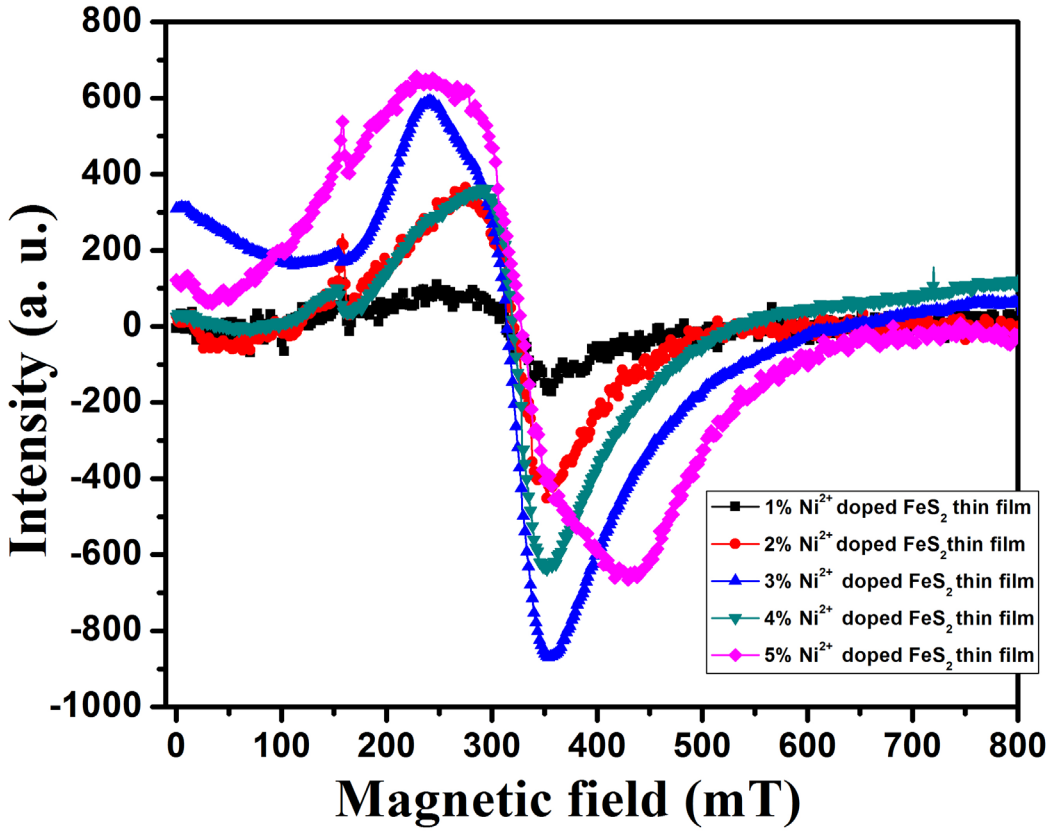
Intensity (a. u.)
Magnetic field (mT)
800
600
400
200
0
-200
-400
-600
-800
-1000
0
100
200
300
400
500
600
700
800
1% Ni2+ doped FeS2 thin film
2% Ni2+ doped FeS2 thin film
3% Ni2+ doped FeS2 thin film
4% Ni2+ doped FeS2 thin film
5% Ni2+ doped FeS2 thin film

Figure 4

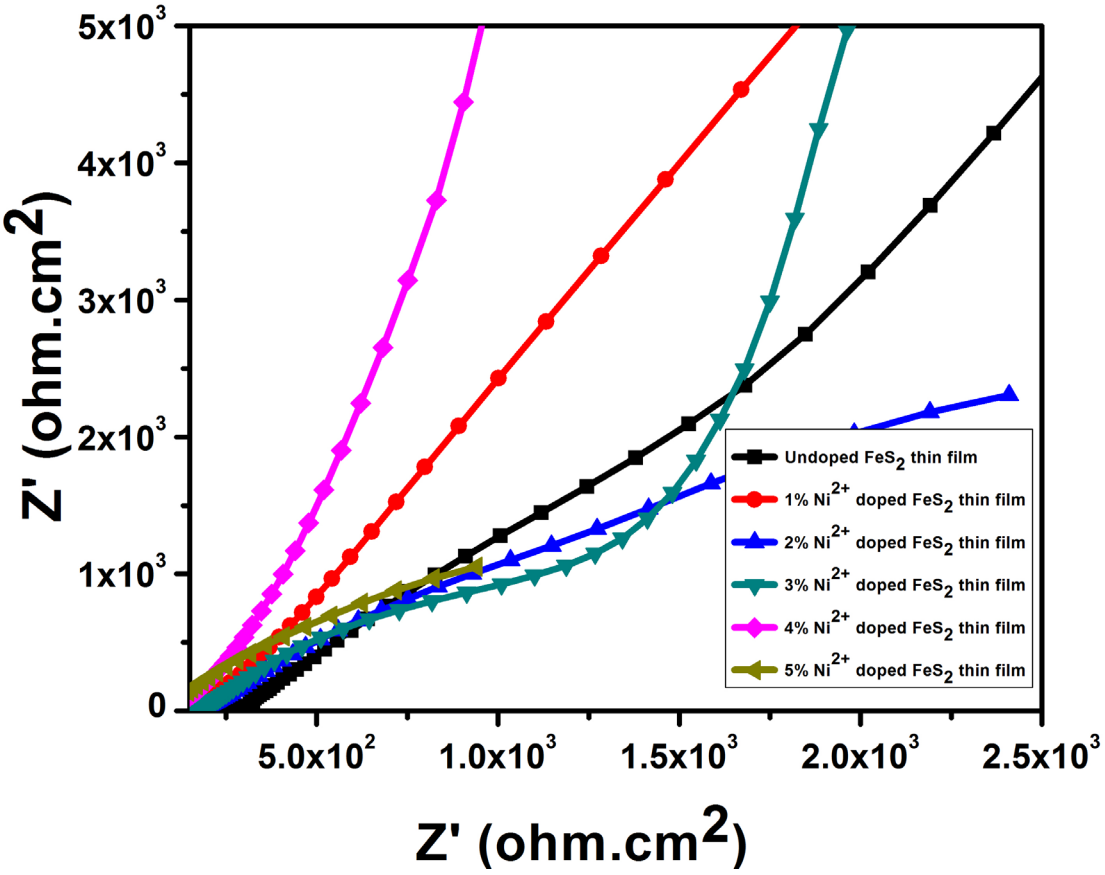
5x10^3
4x10^3
3x10^3
2x10^3
1x10^3
0
Z' (ohm.cm^2)
5.0x10^2
1.0x10^3
1.5x10^3
2.0x10^3
2.5x10^3
Z' (ohm.cm^2)
Undoped FeS2 thin film
1% Ni2+ doped FeS2 thin film
2% Ni2+ doped FeS2 thin film
3% Ni2+ doped FeS2 thin film
4% Ni2+ doped FeS2 thin film
5% Ni2+ doped FeS2 thin film

Figure 5

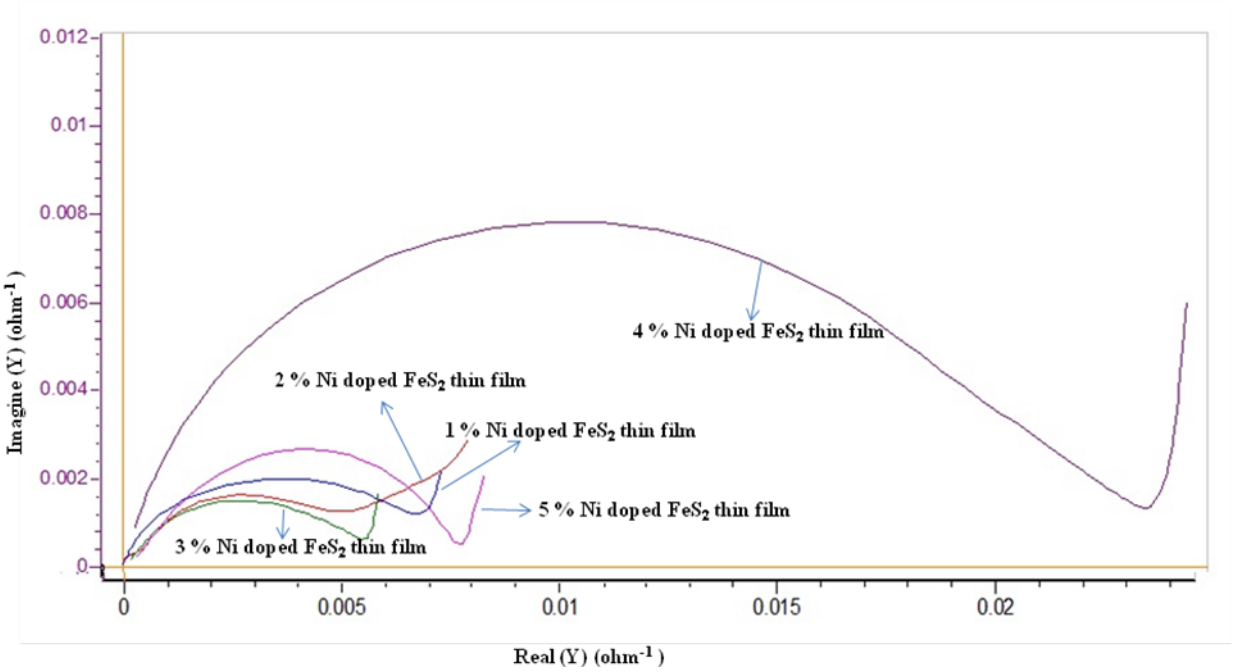
0.012
0.01
0.008
0.006
0.004
0.002
0
Imagine (Y) (ohm-1)
0
0.005
0.01
0.015
0.02
Real (Y) (ohm-1)
4 % Ni doped FeS2 thin film
2 % Ni doped FeS2 thin film
1 % Ni doped FeS2 thin film
5 % Ni doped FeS2 thin film
3 % Ni doped FeS2 thin film

Figure 6

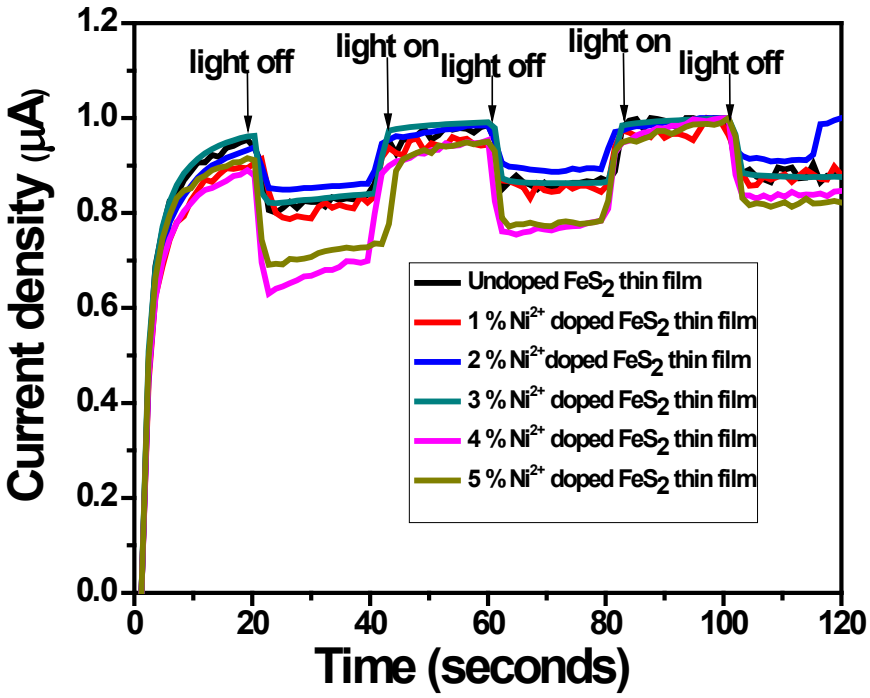
light off
light on
light off
light on
light off
Current density (μA)
Time (seconds)
Undoped FeS2 thin film
1 % Ni2+ doped FeS2 thin film
2 % Ni2+doped FeS2 thin film
3 % Ni2+ doped FeS2 thin film
4 % Ni2+ doped FeS2 thin film
5 % Ni2+ doped FeS2 thin film

Figure 7

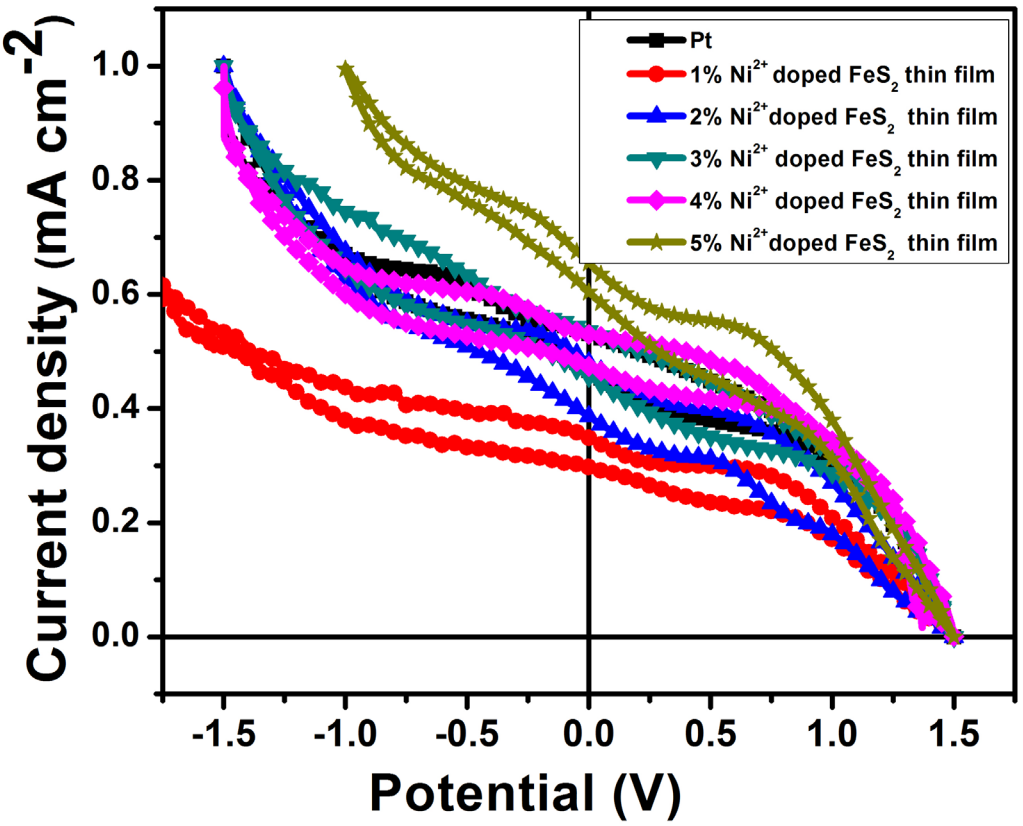
Pt
1% Ni2+ doped FeS2 thin film
2% Ni2+doped FeS2 thin film
3% Ni2+ doped FeS2 thin film
4% Ni2+ doped FeS2 thin film
5% Ni2+doped FeS2 thin film
Current density (mA cm-2)
Potential (V)
1.0
0.8
0.6
0.4
0.2
0.0
-1.5
-1.0
-0.5
0.0
0.5
1.0
1.5

Figure 8

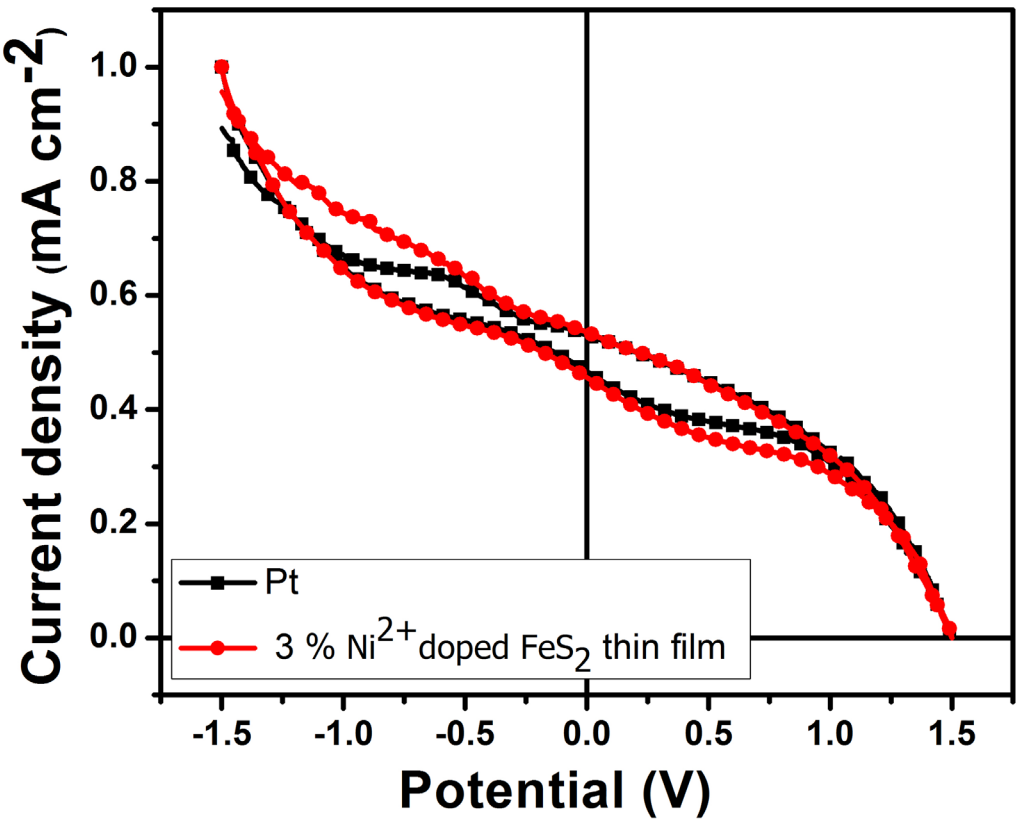
Current density (mA cm-2)
1.0
0.8
0.6
0.4
0.2
0.0
-1.5
-1.0
-0.5
0.0
0.5
1.0
1.5
Potential (V)
Pt
3 % Ni2+doped FeS2 thin film

Figure 9

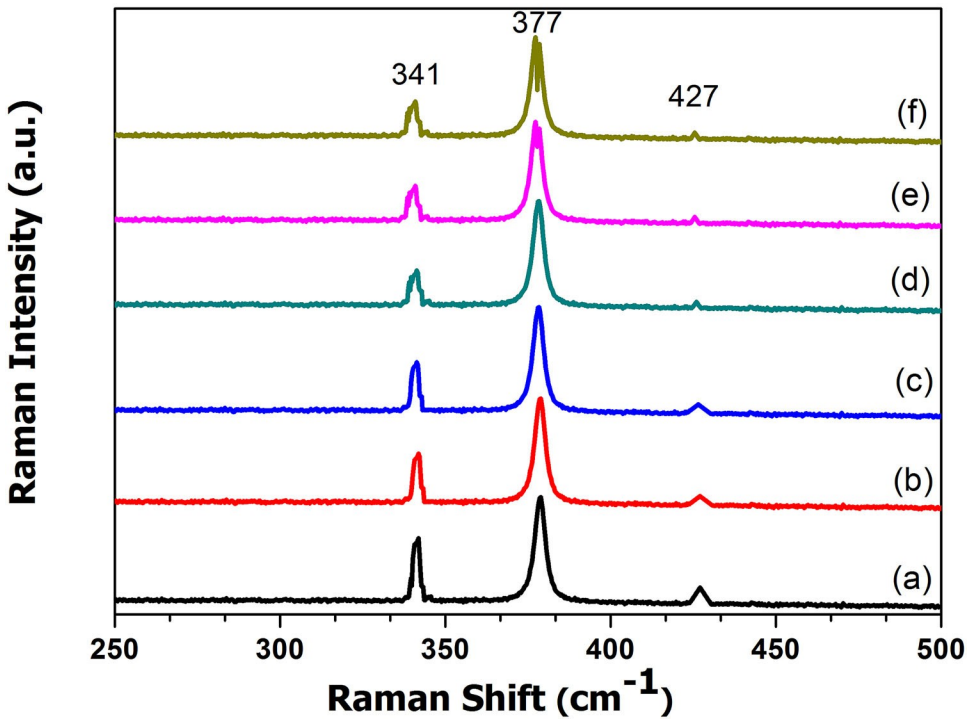
377
341
427
(f)
(e)
(d)
(c)
(b)
(a)
Raman Intensity (a.u.)
250
300
350
400
450
500
Raman Shift (cm-1)

Figure 10

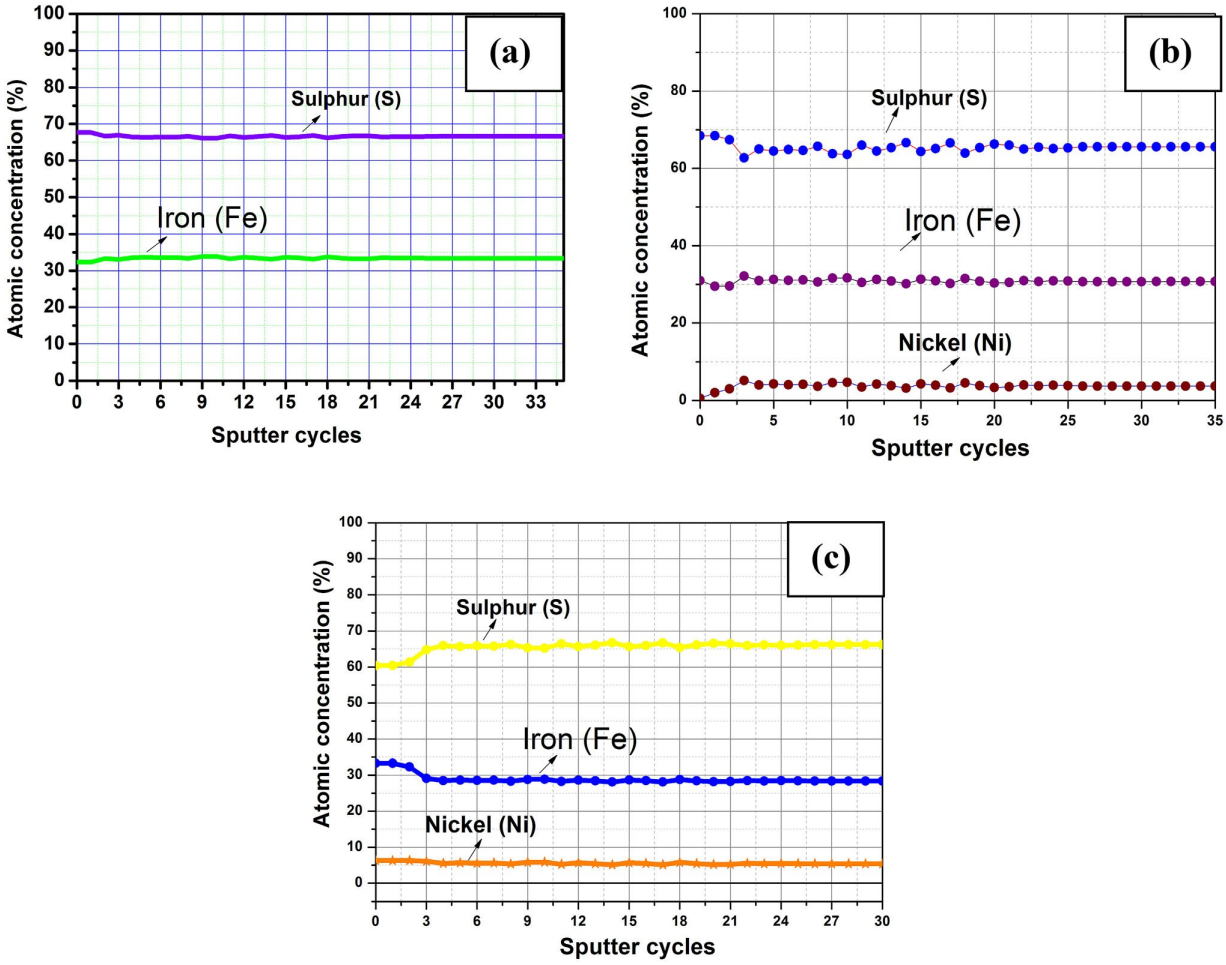
(a)
Sulphur (S)
Iron (Fe)
Atomic concentration (%)
Sputter cycles
(b)
Sulphur (S)
Iron (Fe)
Nickel (Ni)
Atomic concentration (%)
Sputter cycles
(c)
Sulphur (S)
Iron (Fe)
Nickel (Ni)
Atomic concentration (%)
Sputter cycles

Figure 11(a-c)

Table.1

Samples	FWHM of XRD peak (200)	Lattice constants	Crystalline size(nm)	Micro strain ($x10^{-3}$)	Dislocation density ($x10^{24}$ lines/m^2)	No. of crystallites per unit area ($x10^{15}$ m^{-2})
Undoped FeS_2	0.1429	5.3922	101.35	3.42	0.97	2.3
1% Ni^{2+} ions doped FeS_2	0.1091	5.4208	132.55	2.61	0.56	0.9
2% Ni^{2+} ions doped FeS_2	0.0894	5.4208	161.78	2.14	0.38	0.7
3% Ni^{2+} ions doped FeS_2	0.0766	5.4208	188.69	1.83	0.28	0.7
4% Ni^{2+} ions doped FeS_2	0.0759	5.4208	190.71	1.83	0.27	0.8
5% Ni^{2+} ions doped FeS_2	0.0762	5.4208	189.67	1.84	0.28	0.7

Table. 2

Samples	Thickness (nm)	Roughness (nm)	R_s (Ohm.cm^2)	R_b (Ohm.cm^2)	R_{ct} (Ohm.cm^2)
Undoped FeS_2	485	60	311	4660	4349
1% Ni^{2+} ions doped FeS_2	386	102	271	4630	4359
2% Ni^{2+} ions doped FeS_2	420	110	159	789	630
3% Ni^{2+} ions doped FeS_2	497	117	112	181	69
4% Ni^{2+} ions doped FeS_2	520	128	76	380	304
5% Ni^{2+} ions doped FeS_2	572	137	67	220	153

Highlights

- Ni^{2+} doped FeS_2 thin films were attained via a simple electrochemical deposition (ECD) method.
- XRD results confirmed the Ni^{2+} doped FeS_2 thin films.
- 3 mol% Ni^{2+} doped FeS_2 thin film showed enhanced photocurrent-response.
- Ni^{2+} doped FeS_2 is an encouraged material for photoelectrochemical device.